

Measurement of CP Asymmetries and Branching Fractions in
 $B^0 \rightarrow \pi^+\pi^-$, $B^0 \rightarrow K^+\pi^-$, $B^0 \rightarrow \pi^0\pi^0$, $B^0 \rightarrow K^0\pi^0$
and Isospin Analysis of $B \rightarrow \pi\pi$ Decays

The BABAR Collaboration

July 31, 2008

Abstract

We present preliminary results of improved measurements of the CP -violating asymmetries and branching fractions in the decays $B^0 \rightarrow \pi^+\pi^-$, $B^0 \rightarrow K^+\pi^-$, $B^0 \rightarrow \pi^0\pi^0$, and $B^0 \rightarrow K^0\pi^0$. This update includes all data taken at the $\Upsilon(4S)$ resonance by the BABAR experiment at the asymmetric PEP-II B -meson factory at SLAC, corresponding to 467 ± 5 million $B\bar{B}$ pairs. We find

$$\begin{aligned} S_{\pi\pi} &= -0.68 \pm 0.10 \pm 0.03, \\ C_{\pi\pi} &= -0.25 \pm 0.08 \pm 0.02, \\ \mathcal{A}_{K\pi} &= -0.107 \pm 0.016_{-0.004}^{+0.006}, \\ C_{\pi^0\pi^0} &= -0.43 \pm 0.26 \pm 0.05, \\ \mathcal{B}(B^0 \rightarrow \pi^0\pi^0) &= (1.83 \pm 0.21 \pm 0.13) \times 10^{-6}, \\ \mathcal{B}(B^0 \rightarrow K^0\pi^0) &= (10.1 \pm 0.6 \pm 0.4) \times 10^{-6}, \end{aligned}$$

where the first error is statistical and the second is systematic. We observe CP violation with a significance of 6.7σ in $B^0 \rightarrow \pi^+\pi^-$ and 6.1σ in $B^0 \rightarrow K^+\pi^-$. Constraints on the Unitarity Triangle angle α are determined from the isospin relation between all $B \rightarrow \pi\pi$ rates and asymmetries.

Submitted to the 34th International Conference on High-Energy Physics, ICHEP 08,
29 July—5 August 2008, Philadelphia, Pennsylvania, USA.

Stanford Linear Accelerator Center, Stanford University, Stanford, CA 94309

Work supported in part by Department of Energy contract DE-AC03-76SF00515.

The BABAR Collaboration,

B. Aubert, M. Bona, Y. Karyotakis, J. P. Lees, V. Poireau, E. Prencipe, X. Prudent, V. Tisserand
*Laboratoire de Physique des Particules, IN2P3/CNRS et Université de Savoie, F-74941 Annecy-Le-Vieux,
France*

J. Garra Tico, E. Grauges
Universitat de Barcelona, Facultat de Fisica, Departament ECM, E-08028 Barcelona, Spain

L. Lopez^{ab}, A. Palano^{ab}, M. Pappagallo^{ab}
INFN Sezione di Bari^a; Dipartimento di Fisica, Università di Bari^b, I-70126 Bari, Italy

G. Eigen, B. Stugu, L. Sun
University of Bergen, Institute of Physics, N-5007 Bergen, Norway

G. S. Abrams, M. Battaglia, D. N. Brown, R. N. Cahn, R. G. Jacobsen, L. T. Kerth, Yu. G. Kolomensky,
G. Lynch, I. L. Osipenkov, M. T. Ronan,¹ K. Tackmann, T. Tanabe
Lawrence Berkeley National Laboratory and University of California, Berkeley, California 94720, USA

C. M. Hawkes, N. Soni, A. T. Watson
University of Birmingham, Birmingham, B15 2TT, United Kingdom

H. Koch, T. Schroeder
Ruhr Universität Bochum, Institut für Experimentalphysik 1, D-44780 Bochum, Germany

D. Walker
University of Bristol, Bristol BS8 1TL, United Kingdom

D. J. Asgeirsson, B. G. Fulsom, C. Hearty, T. S. Mattison, J. A. McKenna
University of British Columbia, Vancouver, British Columbia, Canada V6T 1Z1

M. Barrett, A. Khan
Brunel University, Uxbridge, Middlesex UB8 3PH, United Kingdom

V. E. Blinov, A. D. Bukin, A. R. Buzykaev, V. P. Druzhinin, V. B. Golubev, A. P. Onuchin,
S. I. Serednyakov, Yu. I. Skovpen, E. P. Solodov, K. Yu. Todyshev
Budker Institute of Nuclear Physics, Novosibirsk 630090, Russia

M. Bondioli, S. Curry, I. Eschrich, D. Kirkby, A. J. Lankford, P. Lund, M. Mandelkern, E. C. Martin,
D. P. Stoker
University of California at Irvine, Irvine, California 92697, USA

S. Abachi, C. Buchanan
University of California at Los Angeles, Los Angeles, California 90024, USA

J. W. Gary, F. Liu, O. Long, B. C. Shen,¹ G. M. Vitug, Z. Yasin, L. Zhang
University of California at Riverside, Riverside, California 92521, USA

¹Deceased

V. Sharma

University of California at San Diego, La Jolla, California 92093, USA

C. Campagnari, T. M. Hong, D. Kovalskyi, M. A. Mazur, J. D. Richman

University of California at Santa Barbara, Santa Barbara, California 93106, USA

T. W. Beck, A. M. Eisner, C. J. Flacco, C. A. Heusch, J. Kroseberg, W. S. Lockman, A. J. Martinez,
T. Schalk, B. A. Schumm, A. Seiden, M. G. Wilson, L. O. Winstrom

University of California at Santa Cruz, Institute for Particle Physics, Santa Cruz, California 95064, USA

C. H. Cheng, D. A. Doll, B. Echenard, F. Fang, D. G. Hitlin, I. Narsky, T. Piatenko, F. C. Porter
California Institute of Technology, Pasadena, California 91125, USA

R. Andreassen, G. Mancinelli, B. T. Meadows, K. Mishra, M. D. Sokoloff

University of Cincinnati, Cincinnati, Ohio 45221, USA

P. C. Bloom, W. T. Ford, A. Gaz, J. F. Hirschauer, M. Nagel, U. Nauenberg, J. G. Smith, K. A. Ulmer,
S. R. Wagner

University of Colorado, Boulder, Colorado 80309, USA

R. Ayad,² A. Soffer,³ W. H. Toki, R. J. Wilson

Colorado State University, Fort Collins, Colorado 80523, USA

D. D. Altenburg, E. Feltresi, A. Hauke, H. Jasper, M. Karbach, J. Merkel, A. Petzold, B. Spaan, K. Wacker
Technische Universität Dortmund, Fakultät Physik, D-44221 Dortmund, Germany

M. J. Kobel, W. F. Mader, R. Nogowski, K. R. Schubert, R. Schwierz, A. Volk

Technische Universität Dresden, Institut für Kern- und Teilchenphysik, D-01062 Dresden, Germany

D. Bernard, G. R. Bonneaud, E. Latour, M. Verderi

Laboratoire Leprince-Ringuet, CNRS/IN2P3, Ecole Polytechnique, F-91128 Palaiseau, France

P. J. Clark, S. Playfer, J. E. Watson

University of Edinburgh, Edinburgh EH9 3JZ, United Kingdom

M. Andreotti^{ab}, D. Bettoni^a, C. Bozzi^a, R. Calabrese^{ab}, A. Cecchi^{ab}, G. Cibinetto^{ab}, P. Franchini^{ab},
E. Luppi^{ab}, M. Negrini^{ab}, A. Petrella^{ab}, L. Piemontese^a, V. Santoro^{ab}

INFN Sezione di Ferrara^a; Dipartimento di Fisica, Università di Ferrara^b, I-44100 Ferrara, Italy

R. Baldini-Ferroli, A. Calcaterra, R. de Sangro, G. Finocchiaro, S. Pacetti, P. Patteri, I. M. Peruzzi,⁴
M. Piccolo, M. Rama, A. Zallo

INFN Laboratori Nazionali di Frascati, I-00044 Frascati, Italy

A. Buzzo^a, R. Contri^{ab}, M. Lo Vetere^{ab}, M. M. Macri^a, M. R. Monge^{ab}, S. Passaggio^a, C. Patrignani^{ab},
E. Robutti^a, A. Santroni^{ab}, S. Tosi^{ab}

INFN Sezione di Genova^a; Dipartimento di Fisica, Università di Genova^b, I-16146 Genova, Italy

²Now at Temple University, Philadelphia, Pennsylvania 19122, USA

³Now at Tel Aviv University, Tel Aviv, 69978, Israel

⁴Also with Università di Perugia, Dipartimento di Fisica, Perugia, Italy

K. S. Chaisanguanthum, M. Morii
Harvard University, Cambridge, Massachusetts 02138, USA

A. Adametz, J. Marks, S. Schenk, U. Uwer
Universität Heidelberg, Physikalisches Institut, Philosophenweg 12, D-69120 Heidelberg, Germany

V. Klose, H. M. Lacker
Humboldt-Universität zu Berlin, Institut für Physik, Newtonstr. 15, D-12489 Berlin, Germany

D. J. Bard, P. D. Dauncey, J. A. Nash, M. Tibbetts
Imperial College London, London, SW7 2AZ, United Kingdom

P. K. Behera, X. Chai, M. J. Charles, U. Mallik
University of Iowa, Iowa City, Iowa 52242, USA

J. Cochran, H. B. Crawley, L. Dong, W. T. Meyer, S. Prell, E. I. Rosenberg, A. E. Rubin
Iowa State University, Ames, Iowa 50011-3160, USA

Y. Y. Gao, A. V. Gritsan, Z. J. Guo, C. K. Lae
Johns Hopkins University, Baltimore, Maryland 21218, USA

N. Arnaud, J. Béquilleux, A. D’Orazio, M. Davier, J. Firmino da Costa, G. Grosdidier, A. Höcker,
V. Lepeltier, F. Le Diberder, A. M. Lutz, S. Pruvot, P. Roudeau, M. H. Schune, J. Serrano, V. Sordini,⁵
A. Stocchi, G. Wormser
*Laboratoire de l’Accélérateur Linéaire, IN2P3/CNRS et Université Paris-Sud 11, Centre Scientifique
d’Orsay, B. P. 34, F-91898 Orsay Cedex, France*

D. J. Lange, D. M. Wright
Lawrence Livermore National Laboratory, Livermore, California 94550, USA

I. Bingham, J. P. Burke, C. A. Chavez, J. R. Fry, E. Gabathuler, R. Gamet, D. E. Hutchcroft, D. J. Payne,
C. Touramanis
University of Liverpool, Liverpool L69 7ZE, United Kingdom

A. J. Bevan, C. K. Clarke, K. A. George, F. Di Lodovico, R. Sacco, M. Sigamani
Queen Mary, University of London, London, E1 4NS, United Kingdom

G. Cowan, H. U. Flaecher, D. A. Hopkins, S. Paramesvaran, F. Salvatore, A. C. Wren
*University of London, Royal Holloway and Bedford New College, Egham, Surrey TW20 0EX, United
Kingdom*

D. N. Brown, C. L. Davis
University of Louisville, Louisville, Kentucky 40292, USA

A. G. Denig, M. Fritsch, W. Gradl, G. Schott
Johannes Gutenberg-Universität Mainz, Institut für Kernphysik, D-55099 Mainz, Germany

⁵Also with Università di Roma La Sapienza, I-00185 Roma, Italy

K. E. Alwyn, D. Bailey, R. J. Barlow, Y. M. Chia, C. L. Edgar, G. Jackson, G. D. Lafferty, T. J. West,
J. I. Yi

University of Manchester, Manchester M13 9PL, United Kingdom

J. Anderson, C. Chen, A. Jawahery, D. A. Roberts, G. Simi, J. M. Tuggle

University of Maryland, College Park, Maryland 20742, USA

C. Dallapiccola, X. Li, E. Salvati, S. Saremi

University of Massachusetts, Amherst, Massachusetts 01003, USA

R. Cowan, D. Dujmic, P. H. Fisher, G. Sciolla, M. Spitznagel, F. Taylor, R. K. Yamamoto, M. Zhao
*Massachusetts Institute of Technology, Laboratory for Nuclear Science, Cambridge, Massachusetts 02139,
USA*

P. M. Patel, S. H. Robertson

McGill University, Montréal, Québec, Canada H3A 2T8

A. Lazzaro^{ab}, V. Lombardo^a, F. Palombo^{ab}

INFN Sezione di Milano^a; Dipartimento di Fisica, Università di Milano^b, I-20133 Milano, Italy

J. M. Bauer, L. Cremaldi, R. Godang,⁶ R. Kroeger, D. A. Sanders, D. J. Summers, H. W. Zhao

University of Mississippi, University, Mississippi 38677, USA

M. Simard, P. Taras, F. B. Viaud

Université de Montréal, Physique des Particules, Montréal, Québec, Canada H3C 3J7

H. Nicholson

Mount Holyoke College, South Hadley, Massachusetts 01075, USA

G. De Nardo^{ab}, L. Lista^a, D. Monorchio^{ab}, G. Onorato^{ab}, C. Sciacca^{ab}

*INFN Sezione di Napoli^a; Dipartimento di Scienze Fisiche, Università di Napoli Federico II^b, I-80126
Napoli, Italy*

G. Raven, H. L. Snoek

*NIKHEF, National Institute for Nuclear Physics and High Energy Physics, NL-1009 DB Amsterdam, The
Netherlands*

C. P. Jessop, K. J. Knoepfel, J. M. LoSecco, W. F. Wang

University of Notre Dame, Notre Dame, Indiana 46556, USA

G. Benelli, L. A. Corwin, K. Honscheid, H. Kagan, R. Kass, J. P. Morris, A. M. Rahimi,

J. J. Regensburger, S. J. Sekula, Q. K. Wong

Ohio State University, Columbus, Ohio 43210, USA

N. L. Blount, J. Brau, R. Frey, O. Igonkina, J. A. Kolb, M. Lu, R. Rahmat, N. B. Sinev, D. Strom,

J. Strube, E. Torrence

University of Oregon, Eugene, Oregon 97403, USA

⁶Now at University of South Alabama, Mobile, Alabama 36688, USA

G. Castelli^{ab}, N. Gagliardi^{ab}, M. Margoni^{ab}, M. Morandin^a, M. Posocco^a, M. Rotondo^a, F. Simonetto^{ab},
R. Stroili^{ab}, C. Voci^{ab}

INFN Sezione di Padova^a; Dipartimento di Fisica, Università di Padova^b, I-35131 Padova, Italy

P. del Amo Sanchez, E. Ben-Haim, H. Briand, G. Calderini, J. Chauveau, P. David, L. Del Buono,
O. Hamon, Ph. Leruste, J. Ocariz, A. Perez, J. Prendki, S. Sitt

*Laboratoire de Physique Nucléaire et de Hautes Energies, IN2P3/CNRS, Université Pierre et Marie
Curie-Paris6, Université Denis Diderot-Paris7, F-75252 Paris, France*

L. Gladney

University of Pennsylvania, Philadelphia, Pennsylvania 19104, USA

M. Biasini^{ab}, R. Covarelli^{ab}, E. Manoni^{ab},

INFN Sezione di Perugia^a; Dipartimento di Fisica, Università di Perugia^b, I-06100 Perugia, Italy

C. Angelini^{ab}, G. Batignani^{ab}, S. Bettarini^{ab}, M. Carpinelli^{ab,7}, A. Cervelli^{ab}, F. Forti^{ab}, M. A. Giorgi^{ab},
A. Lusiani^{ac}, G. Marchiori^{ab}, M. Morganti^{ab}, N. Neri^{ab}, E. Paoloni^{ab}, G. Rizzo^{ab}, J. J. Walsh^a

*INFN Sezione di Pisa^a; Dipartimento di Fisica, Università di Pisa^b; Scuola Normale Superiore di Pisa^c,
I-56127 Pisa, Italy*

D. Lopes Pegna, C. Lu, J. Olsen, A. J. S. Smith, A. V. Telnov

Princeton University, Princeton, New Jersey 08544, USA

F. Anulli^a, E. Baracchini^{ab}, G. Cavoto^a, D. del Re^{ab}, E. Di Marco^{ab}, R. Faccini^{ab}, F. Ferrarotto^a,
F. Ferroni^{ab}, M. Gaspero^{ab}, P. D. Jackson^a, L. Li Gioi^a, M. A. Mazzoni^a, S. Morganti^a, G. Piredda^a,
F. Polci^{ab}, F. Renga^{ab}, C. Voena^a

INFN Sezione di Roma^a; Dipartimento di Fisica, Università di Roma La Sapienza^b, I-00185 Roma, Italy

M. Ebert, T. Hartmann, H. Schröder, R. Waldi

Universität Rostock, D-18051 Rostock, Germany

T. Adye, B. Franek, E. O. Olaiya, F. F. Wilson

Rutherford Appleton Laboratory, Chilton, Didcot, Oxon, OX11 0QX, United Kingdom

S. Emery, M. Escalier, L. Esteve, S. F. Ganzhur, G. Hamel de Monchenault, W. Kozanecki, G. Vasseur,
Ch. Yèche, M. Zito

CEA, Irfu, SPP, Centre de Saclay, F-91191 Gif-sur-Yvette, France

X. R. Chen, H. Liu, W. Park, M. V. Purohit, R. M. White, J. R. Wilson

University of South Carolina, Columbia, South Carolina 29208, USA

M. T. Allen, D. Aston, R. Bartoldus, P. Bechtel, J. F. Benitez, R. Cenci, J. P. Coleman, M. R. Convery,
J. C. Dingfelder, J. Dorfan, G. P. Dubois-Felsmann, W. Dunwoodie, R. C. Field, A. M. Gabareen,
S. J. Gowdy, M. T. Graham, P. Grenier, C. Hast, W. R. Innes, J. Kaminski, M. H. Kelsey, H. Kim, P. Kim,
M. L. Kocian, D. W. G. S. Leith, S. Li, B. Lindquist, S. Luitz, V. Luth, H. L. Lynch, D. B. MacFarlane,
H. Marsiske, R. Messner, D. R. Muller, H. Neal, S. Nelson, C. P. O'Grady, I. Ofte, A. Perazzo, M. Perl,
B. N. Ratcliff, A. Roodman, A. A. Salnikov, R. H. Schindler, J. Schwiening, A. Snyder, D. Su,
M. K. Sullivan, K. Suzuki, S. K. Swain, J. M. Thompson, J. Va'vra, A. P. Wagner, M. Weaver, C. A. West,
W. J. Wisniewski, M. Wittgen, D. H. Wright, H. W. Wulsin, A. K. Yarritu, K. Yi, C. C. Young, V. Ziegler

Stanford Linear Accelerator Center, Stanford, California 94309, USA

⁷Also with Università di Sassari, Sassari, Italy

P. R. Burchat, A. J. Edwards, S. A. Majewski, T. S. Miyashita, B. A. Petersen, L. Wilden
Stanford University, Stanford, California 94305-4060, USA

S. Ahmed, M. S. Alam, J. A. Ernst, B. Pan, M. A. Saeed, S. B. Zain
State University of New York, Albany, New York 12222, USA

S. M. Spanier, B. J. Wogslund
University of Tennessee, Knoxville, Tennessee 37996, USA

R. Eckmann, J. L. Ritchie, A. M. Ruland, C. J. Schilling, R. F. Schwitters
University of Texas at Austin, Austin, Texas 78712, USA

B. W. Drummond, J. M. Izen, X. C. Lou
University of Texas at Dallas, Richardson, Texas 75083, USA

F. Bianchi^{ab}, D. Gamba^{ab}, M. Pelliccioni^{ab}
INFN Sezione di Torino^a; Dipartimento di Fisica Sperimentale, Università di Torino^b, I-10125 Torino, Italy

M. Bomben^{ab}, L. Bosisio^{ab}, C. Cartaro^{ab}, G. Della Ricca^{ab}, L. Lanceri^{ab}, L. Vitale^{ab}
INFN Sezione di Trieste^a; Dipartimento di Fisica, Università di Trieste^b, I-34127 Trieste, Italy

V. Azzolini, N. Lopez-March, F. Martinez-Vidal, D. A. Milanes, A. Oyanguren
IFIC, Universitat de Valencia-CSIC, E-46071 Valencia, Spain

J. Albert, Sw. Banerjee, B. Bhuyan, H. H. F. Choi, K. Hamano, R. Kowalewski, M. J. Lewczuk,
 I. M. Nugent, J. M. Roney, R. J. Sobie
University of Victoria, Victoria, British Columbia, Canada V8W 3P6

T. J. Gershon, P. F. Harrison, J. Ilic, T. E. Latham, G. B. Mohanty
Department of Physics, University of Warwick, Coventry CV4 7AL, United Kingdom

H. R. Band, X. Chen, S. Dasu, K. T. Flood, Y. Pan, M. Pierini, R. Prepost, C. O. Vuosalo, S. L. Wu
University of Wisconsin, Madison, Wisconsin 53706, USA

1 INTRODUCTION

Large CP -violating effects [1] in the B -meson system are among the most remarkable predictions of the Cabibbo–Kobayashi–Maskawa (CKM) quark-mixing model [2]. These predictions have been confirmed in recent years by the *BABAR* and Belle collaborations, both in the interference of B^0 decays to CP eigenstates with and without B^0 – \bar{B}^0 mixing [3–5] and directly, in the interference between the decay amplitudes [6] in $B^0 \rightarrow K^+\pi^-$ [5, 7].

Effective constraints on physics beyond the Standard Model (SM) are provided by high-precision measurements of quantities whose SM predictions suffer only small theoretical uncertainties. Both experimental and theoretical uncertainties often partially cancel out in the determination of CP -violating asymmetries, which makes CP -violation measurements a sensitive probe for effects of yet-undiscovered additional interactions and heavy particles that are introduced by extensions to the SM. All measurements of CP violation to date are in agreement with the indirect predictions from global SM fits [8, 9] that are based on measurements of the magnitudes of the elements of the CKM quark-mixing matrix; this strongly constrains [10] the flavor structure of SM extensions.

The CKM Unitarity Triangle angle $\alpha \equiv \arg[-V_{td}V_{tb}^*/V_{ud}V_{ub}^*]$ is measured through interference between decays with and without B^0 – \bar{B}^0 mixing. Multiple measurements of α , with different decays, further test the consistency of the CKM model. The time-dependent asymmetry in $B^0 \rightarrow \pi^+\pi^-$ is proportional to $\sin 2\alpha$ in the limit that only the $b \rightarrow u$ (“tree”) quark-level amplitude contributes to this decay. In the presence of $b \rightarrow d$ (“penguin”) amplitudes, the time-dependent asymmetry in $B^0 \rightarrow \pi^+\pi^-$ is modified to

$$\begin{aligned}
 a(\Delta t) &= \frac{|\bar{A}(\Delta t)|^2 - |A(\Delta t)|^2}{|\bar{A}(\Delta t)|^2 + |A(\Delta t)|^2} = S_{\pi\pi} \sin(\Delta m_d \Delta t) - C_{\pi\pi} \cos(\Delta m_d \Delta t) \\
 C_{\pi\pi} &= \frac{|A|^2 - |\bar{A}|^2}{|A|^2 + |\bar{A}|^2} \\
 S_{\pi\pi} &= \sqrt{1 - C_{\pi\pi}^2} \sin(2\alpha - 2\Delta\alpha_{\pi\pi}) = \sqrt{1 - C_{\pi\pi}^2} \sin 2\alpha_{\text{eff}},
 \end{aligned} \tag{1}$$

where Δt is the difference between the proper decay times of the signal- and tag-side neutral B mesons and Δm_d is the B^0 mixing frequency. Both the phase difference $\Delta\alpha_{\pi\pi} = \alpha - \alpha_{\text{eff}}$ and the direct CP asymmetry $C_{\pi\pi}$ may differ from zero due to the penguin contribution to the $B^0 \rightarrow \pi^+\pi^-$ decay amplitude A .

The magnitude and relative phase of the penguin contribution to the asymmetry $S_{\pi\pi}$ may be unraveled with an analysis of isospin relations between the $B \rightarrow \pi\pi$ decay amplitudes [11]. The amplitudes A^{ij} of the $B \rightarrow \pi^i\pi^j$ decays and \bar{A}^{ij} of the $\bar{B} \rightarrow \pi^i\pi^j$ decays satisfy the relations

$$\begin{aligned}
 A^{+0} &= \frac{1}{\sqrt{2}}A^{+-} + A^{00}, \\
 \bar{A}^{-0} &= \frac{1}{\sqrt{2}}\bar{A}^{+-} + \bar{A}^{00}.
 \end{aligned} \tag{2}$$

The shape of the corresponding isospin triangle is determined from measurements of the branching fractions and time-integrated CP asymmetries for each of the $B \rightarrow \pi\pi$ decays. No gluonic penguin amplitudes are present in the $\Delta I = 3/2$ decay $B^\pm \rightarrow \pi^\pm\pi^0$, so, neglecting electroweak (EW) penguins, $A^{+0} = \bar{A}^{-0}$. We define the direct CP asymmetry $C_{\pi^0\pi^0}$ in $B^0 \rightarrow \pi^0\pi^0$ as

$$C_{\pi^0\pi^0} = \frac{|A^{00}|^2 - |\bar{A}^{00}|^2}{|A^{00}|^2 + |\bar{A}^{00}|^2}. \tag{3}$$

From the difference in shape of these triangles for the B and \bar{B} decay amplitudes, a constraint on $\Delta\alpha_{\pi\pi}$ can be determined with a four-fold ambiguity.

The phenomenology of the $B \rightarrow \pi\pi$ system has been thoroughly studied in a number of theoretical frameworks and models [12]. Predictions for the relative size and phase of the penguin contribution vary considerably, so increasingly precise measurements will help distinguish among different theoretical approaches and add to our understanding of hadronic B decays.

The measured rates and direct CP -violating asymmetries in $B \rightarrow K\pi$ decays [13–18] reveal puzzling features that could indicate significant contributions from EW penguins [19, 20]. Various methods have been proposed to isolate the Standard Model contribution to this process in order to test for signs of new physics. Sum rules derived from U -spin symmetry relate the rates and asymmetries for the decays B^0 or B^+ to $K^+\pi^-$, $K^+\pi^0$, $K^0\pi^0$, and $K^0\pi^+$ [21], while $SU(3)$ symmetry can be used to make predictions for the $K\pi$ system based on hadronic parameters extracted from the $\pi\pi$ system [19].

2 THE *BABAR* DETECTOR AND DATA SET

The data used in this analysis were collected in 1999–2007 with the *BABAR* detector at the PEP-II asymmetric-energy B -meson factory at the Stanford Linear Accelerator Center. A total of 467 ± 5 million $B\bar{B}$ pairs were used. The preliminary results presented here supersede the results in prior publications [5, 13, 16]. Roughly 22% more $B\bar{B}$ pairs have been added to the *BABAR* data set, and improvements have been introduced to the analysis technique, boosting the signal significance.

In the *BABAR* detector [22], charged particles are detected and their momenta measured by a combination of a five-layer double-sided silicon vertex tracker (SVT) and a 40-layer drift chamber (DCH) that covers 92% of the solid angle in the $\mathcal{T}(4S)$ center-of-mass (c.m.) frame, both operating in a 1.5-T solenoidal magnetic field. Discrimination between charged pions, kaons, and protons is provided by a combination of an internally reflecting ring-imaging Cherenkov detector (DIRC), which covers 84% of the c.m. solid angle in the central region of the *BABAR* detector and has a 91% reconstruction efficiency for pions and kaons with momenta above 1.5 GeV/ c , and the ionization (dE/dx) measurements in the DCH. Neutral-cluster (photon) positions and energies are measured with an electromagnetic calorimeter (EMC) consisting of 6580 CsI(Tl) crystals. The photon energy resolution is $\sigma_E/E = \{2.3/E(\text{GeV})^{1/4} \oplus 1.9\}$ %, and the angular resolution from the interaction point is $\sigma_\theta = 3.9^\circ/\sqrt{E(\text{GeV})}$.

3 ANALYSIS METHOD

Many elements of the measurements discussed in this paper are common to the decay modes $B^0 \rightarrow h^+h'^-(h = \pi \text{ or } K)$, $B^0 \rightarrow \pi^0\pi^0$, and $B^0 \rightarrow K_S^0\pi^0$. The signal B -meson candidates (B_{rec}) are formed by combining two particles, either tracks or π^0 or K_S^0 candidates. The event selection differs for each mode, and is described in detail below.

The number of B decays and the corresponding CP asymmetries are determined in extended unbinned maximum likelihood (M.L.) fits to variables described below. The likelihood is given by the expression

$$\mathcal{L} = \exp\left(-\sum_i^M n_i\right) \prod_j^N \left[\sum_i^M n_i \mathcal{P}_i(\vec{x}_j; \vec{\alpha}_i) \right], \quad (4)$$

where the product is over the number of events N , the sums are over the event categories M , n_i is the coefficient for each category as described below, and the probability-density function (PDF) \mathcal{P} describes the distribution of the variables \vec{x} in terms of parameters $\vec{\alpha}$. The PDF functional forms are discussed in Sec. 3.3.1, 3.3.2, and 3.4.

3.1 Track and K_s^0 Selection

For particle identification in the $B^0 \rightarrow h^+h'^-$ sample, we make use of the track's Cherenkov radiation in the DIRC as well as its ionization energy loss dE/dx in the DCH.

For the DIRC information to be used, we require that each track have the associated Cherenkov angle (θ_C) measured with at least six signal photons detected in the DIRC, where the value of θ_C is required to be within 4.0 standard deviations from either the pion or kaon hypothesis, which effectively removes any candidate containing high-momentum protons. Electrons are explicitly removed based primarily on a comparison of the track momentum and the associated energy deposition in the EMC, with additional information provided by DCH dE/dx and DIRC θ_C measurements.

The ionization energy loss dE/dx in the DCH is used either in combination with DIRC information or alone, which enables a 35% increase in the $B^0 \rightarrow h^+h'^-$ reconstruction efficiency compared to using only the tracks with good DIRC information. A detailed DCH dE/dx calibration that we developed for the $B^0 \rightarrow h^+h'^-$ analysis takes into account variations in the mean value and resolution of dE/dx values with respect to changes in the DCH running conditions over time and the track's charge, polar and azimuthal angles, and number of ionization samples. The calibration is performed with large high-purity samples ($> 10^6$ events) of protons from $\Lambda \rightarrow p\pi^-$, pions and kaons from $D^{*+} \rightarrow D^0\pi^+$ ($D^0 \rightarrow K^-\pi^+$), and $K_s^0 \rightarrow \pi^+\pi^-$ decays that occur in the vicinity of the interaction region.

$K_s^0 \rightarrow \pi^+\pi^-$ candidates are reconstructed from pairs of oppositely charged tracks. The two-track combinations are required to form a vertex with a χ^2 probability greater than 0.001 and a $\pi^+\pi^-$ invariant mass within 11.2 MeV/ c^2 (3.7σ) of the K_s^0 mass [23].

3.2 π^0 Selection

We form $\pi^0 \rightarrow \gamma\gamma$ candidates from pairs of clusters in the EMC that are isolated from any charged tracks. Clusters are required to have a transverse energy deposition consistent with that of a photon and to have an energy $E_\gamma > 30$ MeV for $B^0 \rightarrow \pi^0\pi^0$ and $E_\gamma > 50$ MeV for $B^0 \rightarrow K_s^0\pi^0$. We use π^0 candidates that fall within the invariant-mass range $110 < m_{\gamma\gamma} < 160$ MeV/ c^2 .

For the $B^0 \rightarrow \pi^0\pi^0$ sample, we also use π^0 candidates from a single EMC cluster containing two adjacent photons (a merged π^0), or one EMC cluster and two tracks from a photon conversion to an e^+e^- pair inside the detector. To reduce the background from random photon combinations, the angle θ_γ between the photon momentum vector in the π^0 rest frame and the π^0 momentum vector in the laboratory frame is required to satisfy $|\cos\theta_\gamma| < 0.95$. The π^0 candidates are fitted kinematically with their mass constrained to the nominal π^0 mass [23].

Photon conversions are selected from pairs of oppositely charged tracks with an invariant mass below 30 MeV/ c^2 whose combined momentum vector points straight away from the beam spot. The conversion point is required to lie inside the detector material. Converted photons are combined with photons from single EMC clusters to form π^0 candidates.

Single EMC clusters containing two photons are selected with the transverse second moment, $S = \sum_i E_i \times (\Delta\alpha_i)^2/E$, where E_i is the energy in each CsI(Tl) crystal and $\Delta\alpha_i$ is the angle

between the cluster centroid and the crystal. The second moment is used to distinguish merged π^0 candidates from both single photons and neutral hadrons.

3.3 Event Selection in $B^0 \rightarrow \pi^+\pi^-$, $B^0 \rightarrow K^+\pi^-$, and $B^0 \rightarrow \pi^0\pi^0$

Two kinematic variables are used in the $B^0 \rightarrow h^+h'^-$ and $B^0 \rightarrow \pi^0\pi^0$ analyses to separate B -meson decays from the large $e^+e^- \rightarrow q\bar{q}$ ($q = u, d, s, c$) combinatoric background [22]. One is the beam-energy-substituted mass $m_{\text{ES}} = \sqrt{(s/2 + \mathbf{p}_i \cdot \mathbf{p}_B)^2/E_i^2 - \mathbf{p}_B^2}$, where \sqrt{s} is the total e^+e^- c.m. energy, (E_i, \mathbf{p}_i) is the four-momentum of the initial e^+e^- system in the laboratory frame, and \mathbf{p}_B is the laboratory momentum of the B candidate. The other is $\Delta E = E_B^* - \sqrt{s}/2$, where E_B^* is the B candidate's energy in the c.m. frame.

Two additional quantities take advantage of the event topology to further separate B decays from the $q\bar{q}$ background. The absolute value of the cosine of the angle θ_s between the sphericity axes [24] of the B candidate's decay products and that of the remaining tracks and neutral clusters in the event, computed in the c.m. frame, is peaked at 1.0 for the jet-like $q\bar{q}$ events but has a flat distribution for B decays. We require $|\cos \theta_s| < 0.7$ for $B^0 \rightarrow \pi^0\pi^0$ and $|\cos \theta_s| < 0.91$ for $B^0 \rightarrow h^+h'^-$. For the $B^0 \rightarrow h^+h'^-$ sample, we further require that the second Fox–Wolfram moment [26] satisfy $R_2 < 0.7$ to remove a small remaining background from $e^+e^- \rightarrow \tau^+\tau^-$ events.

To improve the discrimination against $q\bar{q}$ events, a Fisher discriminant \mathcal{F} is formed as a linear combination of the sums $L_0 \equiv \sum_i |\mathbf{p}_i^*|$ and $L_2 \equiv \sum_i |\mathbf{p}_i^*| \cos^2 \theta_i^*$, where \mathbf{p}_i^* are the momenta and θ_i^* are the angles with respect to the thrust axis [25] of the B candidate, both in the c.m. frame, of all tracks and clusters not used to reconstruct the signal B -meson candidate. In the case of $B^0 \rightarrow \pi^0\pi^0$, we improve the sensitivity of the signal by combining \mathcal{F} with three other quantities in a neural network. These are the $|\cos \theta_s|$ described above, $|\cos \theta_B|$, where θ_B is the angle between the center-of-mass momentum vector of the signal B and the beam axis, and $|\cos \theta_T|$, where θ_T is the angle between the thrust axis of the signal B -meson's daughters and the beam axis.

3.3.1 $B^0 \rightarrow \pi^+\pi^-$ and $B^0 \rightarrow K^+\pi^-$

We reconstruct candidate decays $B_{\text{rec}} \rightarrow h^+h'^-$ from pairs of oppositely charged tracks in the polar-angle range $0.35 < \theta_{\text{lab}} < 2.40$ that are consistent with originating from a common decay point with a χ^2 probability of at least 0.001. The remaining particles are examined to infer whether the other B meson in the event (B_{tag}) decayed as a B^0 or \bar{B}^0 (flavor tag). We perform an unbinned extended M.L. fit to separate $B^0 \rightarrow \pi^+\pi^-$ and $B^0 \rightarrow K^+\pi^-$ decays and determine simultaneously their CP -violating asymmetries $S_{\pi\pi}$, $C_{\pi\pi}$, and $\mathcal{A}_{K\pi}$ and the signal and background yields and PDF parameters. The fit uses particle-identification, kinematic, event-shape, B_{tag} flavor, and Δt information.

The variables m_{ES} and ΔE are calculated assuming that both tracks are charged pions. The $B^0 \rightarrow \pi^+\pi^-$ events are described by a Gaussian distribution for both m_{ES} and ΔE , where the resolutions are found to be 2.6 MeV/ c^2 and 29 MeV, respectively. For each kaon in the final state, the ΔE peak position is shifted from zero by an amount that depends on the kaon momentum, with an average shift of -45 MeV. We require $m_{\text{ES}} > 5.20$ GeV/ c^2 and $|\Delta E| < 0.150$ GeV. The large region below the signal in m_{ES} effectively determines the background shape parameters, while the wide range in ΔE allows us to separate B^0 decays to all four final states ($\pi^+\pi^-$, $K^+\pi^-$, π^+K^- , and K^+K^-) in a single fit.

We construct θ_C PDFs for the pion and kaon hypotheses, and dE/dx PDFs for the pion, kaon,

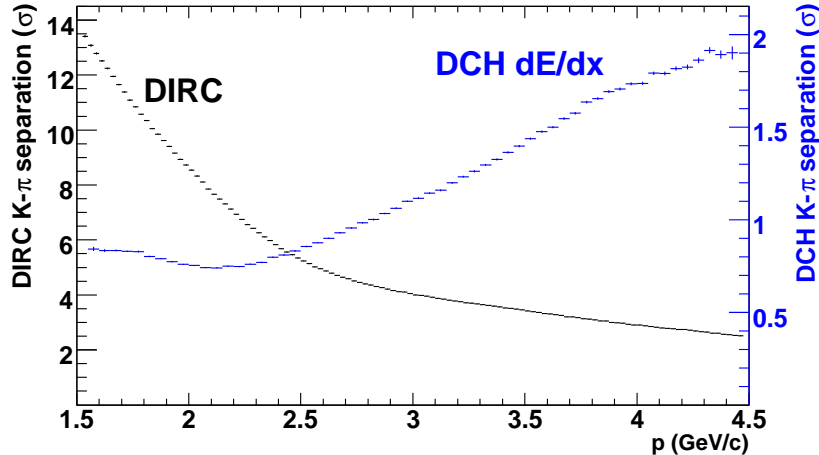


Figure 1: The average difference between the expected values of DIRC θ_C and DCH dE/dx for pions and kaons at $0.35 < \theta_{\text{lab}} < 2.40$, divided by the uncertainty, as a function of laboratory momentum in $B^0 \rightarrow K^+\pi^-$ decays in *BABAR*.

Table 1: Average tagging efficiency ϵ , average mistag fraction w , mistag fraction difference $\Delta w = w(B^0) - w(\bar{B}^0)$, and effective tagging efficiency Q for signal events in each tagging category. The quantities are measured in the large-statistics B_{flav} sample of fully reconstructed neutral B -meson decays.

Category	ϵ (%)	w (%)	Δw (%)	Q (%)
Lepton	8.96 ± 0.07	2.9 ± 0.3	0.2 ± 0.5	7.95 ± 0.11
Kaon I	10.81 ± 0.07	5.3 ± 0.3	0.0 ± 0.6	8.64 ± 0.14
Kaon II	17.18 ± 0.09	14.5 ± 0.3	0.4 ± 0.6	8.64 ± 0.17
KaonPion	13.67 ± 0.08	23.3 ± 0.4	-0.6 ± 0.7	3.91 ± 0.12
Pion	14.19 ± 0.08	32.6 ± 0.4	5.1 ± 0.7	1.73 ± 0.09
Other	9.55 ± 0.07	41.5 ± 0.5	3.8 ± 0.8	0.28 ± 0.04
Total				31.1 ± 0.3

and proton hypotheses, separately for each charge. The $K-\pi$ separations provided by θ_C and dE/dx are complementary: for θ_C , the separation varies from 2.5σ at $4.5 \text{ GeV}/c$ to 13σ at $1.5 \text{ GeV}/c$, while for dE/dx it varies from less than 1.0σ at $1.5 \text{ GeV}/c$ to 1.9σ at $4.5 \text{ GeV}/c$ (Fig. 1). For more details, please see Ref. [5].

We use a multivariate technique [27] to determine the flavor of B_{tag} . Separate neural networks are trained to identify leptons and kaons from B and D decays and soft pions from D^* decays. Events are assigned to one of seven mutually exclusive tagging categories (including untagged events) based on the estimated average mistag probability and the source of the tagging information. The quality of tagging is expressed in terms of the effective efficiency $Q = \sum_k \epsilon_k (1 - 2w_k)^2$, where ϵ_k and w_k are the efficiencies and mistag probabilities, respectively, for events tagged in category k . The difference in mistag probabilities is given by $\Delta w = w_{B^0} - w_{\bar{B}^0}$. Table 1 summarizes the tagging performance measured in a large data sample of fully reconstructed neutral B_{flav} decays to $D^{(*)-}(\pi^+, \rho^+, a_1^+)$.

The time difference $\Delta t = \Delta z/\beta\gamma c$ is obtained from the known boost of the e^+e^- system ($\beta\gamma = 0.56$) and the measured distance Δz along the beam (z) axis between the B_{rec} and B_{tag} decay vertices. A description of the inclusive reconstruction of the B_{tag} vertex is given in [28]. We require $|\Delta t| < 20$ ps and $\sigma_{\Delta t} < 2.5$ ps, where $\sigma_{\Delta t}$ is the error on Δt determined separately for each event. The signal Δt PDF for $B^0 \rightarrow \pi^+\pi^-$ is given by

$$f_k^\pm(\Delta t_{\text{meas}}) = \frac{e^{-|\Delta t|/\tau}}{4\tau} \left\{ (1 \mp \Delta w) \pm (1 - 2w_k) [S_{\pi\pi} \sin(\Delta m_d \Delta t) - C_{\pi\pi} \cos(\Delta m_d \Delta t)] \right\} \otimes R(\Delta t_{\text{meas}} - \Delta t), \quad (5)$$

where f_k^+ (f_k^-) indicates a B^0 (\bar{B}^0) flavor tag and the index k indicates the tagging category. The resolution function $R(\Delta t_{\text{meas}} - \Delta t)$ for signal candidates is a sum of three Gaussian functions, identical to the one described in Ref. [28], with parameters determined from a fit to the B_{flav} sample (including events in all seven tagging categories). The background Δt distribution is also modeled as the sum of three Gaussians, where the common parameters used to describe the background shape for all tagging categories are determined simultaneously with the CP parameters in the maximum likelihood fit.

The M.L. fit includes 28 components: B^0 signal decays and background with the final states $\pi^+\pi^-$, $K^+\pi^-$, $K^-\pi^+$, and K^+K^- where either the positively charged or the negatively charged track, or both, have good DIRC information ($2 \times 4 \times 3 = 24$ components) plus the $p\pi^-$, pK^- , $\pi^+\bar{p}$ and $K^+\bar{p}$ background components where the (anti)proton has no DIRC information. The $K^\pm\pi^\mp$ event yields are parameterized as $n_{K^\pm\pi^\mp} = n_{K\pi} (1 \mp \mathcal{A}_{K\pi}^{\text{raw}})/2$. All other coefficients are products of the fraction of events in each tagging category, taken from B_{flav} events, and the event yield. The background PDFs are a threshold function [29] for m_{ES} and a second-order polynomial for ΔE . The \mathcal{F} PDF is a sum of two asymmetric Gaussians for both the signal and background. We used large samples of simulated B decays to investigate the effects of backgrounds from other B decays on the determination of the CP -violating asymmetries in $B^0 \rightarrow \pi^+\pi^-$ and $B^0 \rightarrow K^+\pi^-$ and determined them to be negligible.

3.3.2 $B^0 \rightarrow \pi^0\pi^0$

$B^0 \rightarrow \pi^0\pi^0$ events are identified with an M.L. fit to the variables m_{ES} , ΔE , and NN , the output of the event-shape neural network. We require $m_{\text{ES}} > 5.20$ GeV/ c^2 and $|\Delta E| < 0.2$ GeV. Tails in the EMC response produce a correlation between m_{ES} and ΔE , so a two-dimensional PDF, derived from detailed Monte Carlo (MC) simulation, is used to describe signal. The NN distribution is binned in ten bins (equally populated for signal) and described by a parametric step-function PDF with 9 height parameters taken from the MC and fixed in the fit. B_{flav} data are used to verify that the MC accurately reproduces the NN distribution. The $q\bar{q}$ background PDFs are a threshold function [29] for m_{ES} , a second-order polynomial for ΔE , and a parametric step function for NN . For $q\bar{q}$ events, NN is not distributed uniformly across the bins but rises sharply toward the highest bins. We see a small linear correlation between the shape parameter of the m_{ES} threshold function and the NN bin number, and this linear relation is taken into account in the fit. All $q\bar{q}$ background PDF parameters are allowed to float in the M.L. fit.

The decays $B^+ \rightarrow \rho^+\pi^0$ and $B^0 \rightarrow K_S^0\pi^0$ ($K_S^0 \rightarrow \pi^0\pi^0$) add 71 ± 10 background events to $B^0 \rightarrow \pi^0\pi^0$ and are included as an additional fixed component in the M.L. fit. We model these B -

decay backgrounds with a two-dimensional PDF to describe m_{ES} and ΔE , and with a step function for NN , all taken from MC simulation.

The time-integrated CP asymmetry is measured by the B -flavor tagging algorithm described previously. The fraction of events in each tagging category is also constrained to the corresponding fraction determined from MC simulation. The PDF coefficient for the $B^0 \rightarrow \pi^0\pi^0$ signal is given by the expression

$$n_{\pi^0\pi^0,k} = \frac{1}{2}f_k N_{\pi^0\pi^0} \left\{ 1 - s_j(1 - 2\chi)(1 - 2w_k)C_{\pi^0\pi^0} \right\}, \quad (6)$$

where f_k is the fraction of events in the tagging category k , $N_{\pi^0\pi^0}$ is the number of $B^0 \rightarrow \pi^0\pi^0$ decays, $\chi = 0.188 \pm 0.003$ [23] is the time-integrated B^0 mixing probability, and $s_j = +1(-1)$ when the B_{tag} is a B^0 (\bar{B}^0).

3.4 $B^0 \rightarrow K^0\pi^0$

For each $B^0 \rightarrow K_S^0\pi^0$ candidate, two independent kinematic variables are computed. The first one is m_B , the invariant mass of the reconstructed B meson, B_{rec} . The second one is m_{miss} , the invariant mass of the other B , B_{tag} , computed from the known beam energy, by applying a mass constraint to B_{rec} [30]. For signal decays, m_B and m_{miss} peak near the B^0 mass with resolutions of $\sim 36 \text{ MeV}/c^2$ and $\sim 5.3 \text{ MeV}/c^2$, respectively. Both the m_{miss} and m_B distributions exhibit a low-side tail due to the leakage of energy deposits out of the EMC. We select candidates within the ranges $5.11 < m_{\text{miss}} < 5.31 \text{ GeV}/c^2$ and $5.13 < m_B < 5.43 \text{ GeV}/c^2$, which include a signal peak and a ‘‘sideband’’ region for background characterization. In the events with more than one reconstructed candidate (0.8% of the total), we select the candidate with the smallest $\chi^2 = \sum_{i=\pi^0, K_S^0} (m_i - m'_i)^2 / \sigma_{m_i}^2$, where m_i (m'_i) is the measured (nominal) mass and σ_{m_i} is the estimated uncertainty on the measured mass of particle i .

We exploit topological observables, computed in the c.m. frame, to discriminate jet-like $e^+e^- \rightarrow q\bar{q}$ events ($q = u, d, s, c$) from the nearly spherical $B\bar{B}$ events. In order to reduce the number of background events, we require $L_2/L_0 < 0.55$, where $L_j \equiv \sum_i |\mathbf{p}_i^*| \cos^j \theta_i^*$ and θ_i^* are computed with respect to the sphericity axis [24] of the B_{rec} candidate. We compute $\cos \theta_B^*$, the cosine of the angle between the direction of the B meson and the nominal direction of the magnetic field (z axis). This variable is distributed as $1 - \cos^2 \theta_B^*$ for signal events and is nearly flat for background events. We select events with $|\cos \theta_B^*| < 0.9$. We also use the distributions of L_2/L_0 and $\cos \theta_B^*$ to discriminate the signal from the residual background in a M.L. fit. Using a full detector simulation, we estimate that our selection retains $(34.2 \pm 1.2)\%$ of the signal events, where the error includes both statistical and systematic contributions. The selected sample of $B^0 \rightarrow K_S^0\pi^0$ candidates is dominated by random $K_S^0\pi^0$ combinations from $e^+e^- \rightarrow q\bar{q}$ fragmentation. Using large samples of simulated $B\bar{B}$ events, we find that backgrounds from other B -meson decays are small, $\mathcal{O}(0.1\%)$; however, we study in detail the effect of a number of specific B decay channels. The dominant ones are $B^+ \rightarrow \rho^+ K_S^0$, $B^+ \rightarrow K^{*+}\pi^0$, and $B^+ \rightarrow K_S^0\pi^0\pi^+$, and we include this effect in our study of the systematic errors.

For the $B^0 \rightarrow K_S^0\pi^0$ decay, where no charged particles are present at the decay vertex, we compute the decay point of the B_{rec} using the knowledge of the K_S^0 trajectory from the measurement of $\pi^+\pi^-$ momenta and the knowledge of the average interaction point [31].

We extract the signal yield from an extended unbinned M.L. fit to kinematic, event-shape, flavor-tag, and decay-time quantities. The use of tagging and decay-time information in the M.L. fit further improves discrimination between signal and background. We have verified that all

correlations are negligible, and so construct the likelihood function as a product of one-dimensional PDFs. Residual correlations are taken into account in the systematic uncertainty, as explained below.

The PDFs for signal events are parameterized based on a large sample of fully reconstructed B decays in data and from simulated events. For background PDFs, we select the functional form from the background-dominated sideband regions in the data.

The likelihood function is defined as:

$$\begin{aligned} \mathcal{L}(S_f, C_f, N_{\text{sig}}, N_{\text{bkg}}, f_{\text{sig}}, f_{\text{bkg}}, \vec{\alpha}) &= \frac{e^{-(N_{\text{sig}}+N_{\text{bkg}})}}{N!} \\ &\times \prod_{i \in g} [N_{\text{sig}} f_{\text{sig}} \epsilon_{\text{sig}}^c \mathcal{P}_{\text{sig}}(\vec{x}_i, \vec{y}_i; S_f, C_f) + N_{\text{bkg}} f_{\text{bkg}} \epsilon_{\text{bkg}}^c \mathcal{P}_{\text{bkg}}(\vec{x}_i, \vec{y}_i; \vec{\alpha})] \\ &\times \prod_{i \in b} [N_{\text{sig}} (1 - f_{\text{sig}}) \epsilon_{\text{sig}}^c \mathcal{P}'_{\text{sig}}(\vec{x}_i; C_f) + N_{\text{bkg}} (1 - f_{\text{bkg}}) \epsilon_{\text{bkg}}^c \mathcal{P}'_{\text{bkg}}(\vec{x}_i; \vec{\alpha})], \end{aligned} \quad (7)$$

where the N selected events are partitioned into two subsets: $i \in g$ events have Δt information, while $i \in b$ events do not. Here, f_{sig} (f_{bkg}) is the fraction of signal (background) events $\in g$, and $1 - f_{\text{sig}}$ ($1 - f_{\text{bkg}}$) is the fraction of events $\in b$. The probabilities \mathcal{P}_{sig} and \mathcal{P}_{bkg} are products of PDFs for signal (sig) and background (bkg) hypotheses evaluated for the measurements $\vec{x}_i = \{m_B, m_{\text{miss}}, L_2/L_0, \cos \theta_B^*, \text{flavor tag, tagging category}\}$ and $\vec{y}_i = \{\Delta t, \sigma_{\Delta t}\}$. $\mathcal{P}'_{\text{sig}}$ and $\mathcal{P}'_{\text{bkg}}$ are the corresponding probabilities for events without Δt information. In the formula, $\vec{\alpha}$ represents the set of parameters that define the shape of the PDFs. Along with the CP asymmetries S_f and C_f , the fit extracts the yields N_{sig} and N_{bkg} , the fraction of events f_{sig} and f_{bkg} , and the parameters $\vec{\alpha}$ that describe the background PDFs.

4 RESULTS AND SYSTEMATIC UNCERTAINTIES

4.1 $B^0 \rightarrow \pi^0 \pi^0$ Results

Results from the M.L. fit for the $B^0 \rightarrow \pi^0 \pi^0$ decay mode are summarized in Table 2. Distributions of m_{ES} , ΔE , and NN for $B^0 \rightarrow \pi^0 \pi^0$ are shown in Fig. 2, where a weighting and background-subtraction technique, *sPlots* [32], is used to display the signal events. The same technique is used to display the $q\bar{q}$ background as well, shown in the insets.

The uncertainty in the efficiency for the $B^0 \rightarrow \pi^0 \pi^0$ decay mode is dominated by a 3% systematic uncertainty per π^0 , estimated from a study of $\tau \rightarrow \pi \pi^0 \nu_\tau$ decays. There is an additional 1.0% uncertainty in the resolution of the signal shape and a 0.45% uncertainty due to the limited knowledge of the m_{ES} and ΔE peak positions in data, estimated by shifting the m_{ES} and ΔE

Table 2: Results for the $B^0 \rightarrow \pi^0 \pi^0$ and $B^0 \rightarrow K^0 \pi^0$ decay modes: signal yields N_{sig} , efficiencies, branching fractions, and time-integrated CP asymmetries. When two uncertainties are given, the first is statistical and the second systematic.

	N_{sig}	Efficiency	Branching fraction	Asymmetry
$B^0 \rightarrow \pi^0 \pi^0$	247 ± 29	$(28.8 \pm 1.8)\%$	$(1.83 \pm 0.21 \pm 0.13) \times 10^{-6}$	$-0.43 \pm 0.26 \pm 0.05$
$B^0 \rightarrow K_S^0 \pi^0$	556 ± 32	$(34.2 \pm 1.2)\%$	$(10.1 \pm 0.6 \pm 0.4) \times 10^{-6}$	[33]

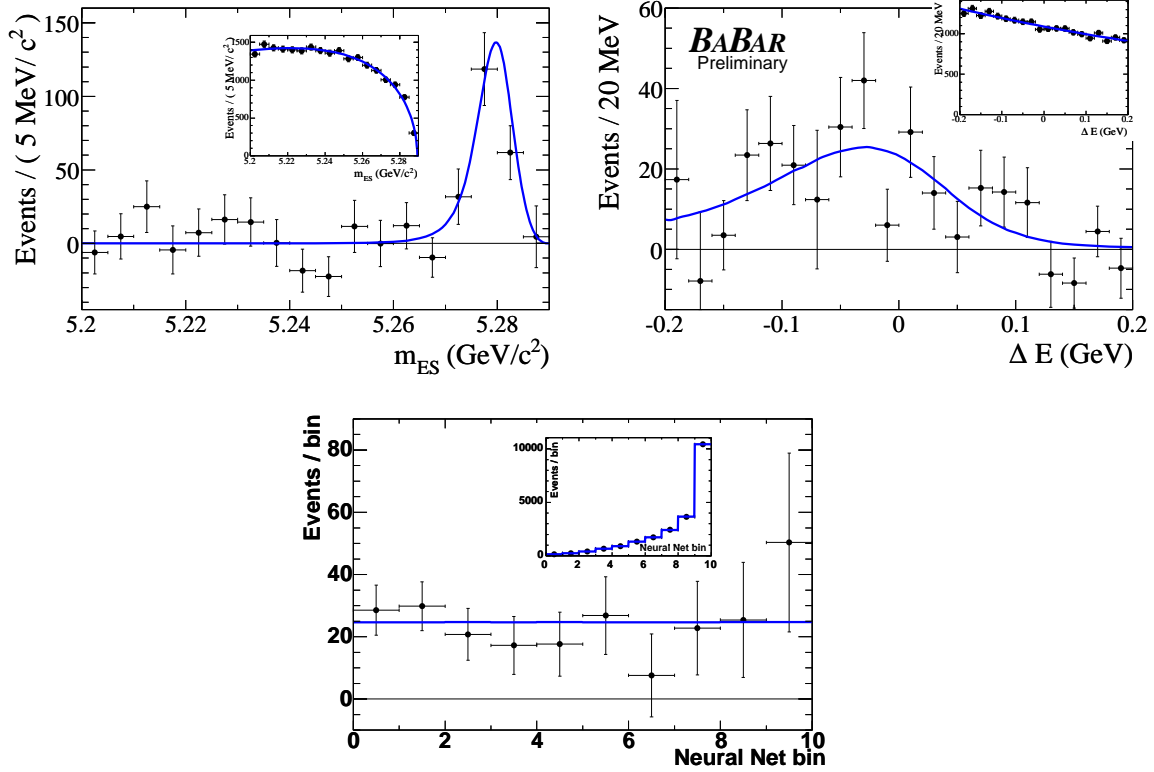


Figure 2: s Plots for $B^0 \rightarrow \pi^0\pi^0$ signal (background shown in the inset plots): (top left) m_{ES} , (top right) ΔE , (bottom) the binned NN. The line in each plot shows the corresponding PDF.

means and resolutions by amounts determined from MC–data comparison in a control sample of $B^+ \rightarrow \pi^+\pi^0$ events. We also take an uncertainty of 1.5%, determined from the B_{flav} sample, due to the $|\cos\theta_S|$ requirement. Systematic uncertainties involving the M.L. fit are evaluated by varying the PDF parameters and refitting the data. These contribute an uncertainty of 8.3 events to the branching-fraction measurement and an uncertainty of 0.05 to $C_{\pi^0\pi^0}$. The various systematics sources are tabulated in Table 3.

4.2 $B^0 \rightarrow \pi^+\pi^-$ and $B^0 \rightarrow K^+\pi^-$ Results

Results for the $B^0 \rightarrow h^+h'^-$ decay modes are listed in Table 4. The correlation coefficient between $S_{\pi\pi}$ and $C_{\pi\pi}$ is found to be -0.056 , and the correlation between $C_{\pi\pi}$ and $\mathcal{A}_{K\pi}$ is 0.019 . In Fig. 3, we show s Plots for m_{ES} , ΔE , and \mathcal{F} for the $B^0 \rightarrow h^+h'^-$ signal and background. The direct CP asymmetry in $B^0 \rightarrow K^+\pi^-$ is apparent in the distribution of ΔE plotted separately for B^0 and \bar{B}^0 decays, shown in Fig. 4. We show the distributions of Δt for $B^0 \rightarrow K^\pm\pi^\mp$ signal and background decays in Fig. 5. In Fig. 6, we show the distribution of Δt separately for $B^0 \rightarrow \pi^+\pi^-$ events tagged as B^0 or \bar{B}^0 , and the asymmetry $a(\Delta t)$. The central values and errors for $S_{\pi\pi}$ and $C_{\pi\pi}$ are shown in Fig. 7, along with confidence-level contours corresponding to statistical significances ranging from 1 to 7 standard deviations. Our measurement excludes the absence of CP violation in $B^0 \rightarrow \pi^+\pi^-$ ($S_{\pi\pi} = 0$, $C_{\pi\pi} = 0$) at a confidence level of 2×10^{-11} , or 6.7σ (where systematic errors are taken into account).

Table 3: Systematic uncertainties in the determination of the $B^0 \rightarrow \pi^0\pi^0$ signal yield ($N_{\pi^0\pi^0}$) and branching fraction, and the direct CP asymmetry $C_{\pi^0\pi^0}$. The total branching-fraction systematic is the sum in quadrature of the uncertainties on the signal yield, the signal efficiency, and the B -meson counting.

Source	$N_{\pi^0\pi^0}$	$\sigma_{\text{syst}}(\mathcal{B})/\mathcal{B}$	$C_{\pi^0\pi^0}$
Peaking background	± 4.9		± 0.030
Tagging	± 0.35		± 0.034
Background shape	± 5.5		± 0.023
Signal shape	± 3.8		± 0.020
Total fit systematics	± 8.3	3.4%	± 0.055
π^0 efficiency		6.0%	
$ \cos\theta_s $ selection		1.5%	
neutrals resolution		1.0%	
m_{ES} and ΔE shape		0.5%	
Total efficiency systematics		6.3%	
Number of $B\bar{B}$ pairs		1.1%	
Total systematic error		7.2%	± 0.055

Table 4: Results for the $B^0 \rightarrow h^+h'^-$ decay modes. For each mode, the number of signal events N_{sig} and CP asymmetries are shown. Statistical, followed by systematic, uncertainties are given for the asymmetries.

Mode	N_{sig}	Asymmetry
$B^0 \rightarrow \pi^+\pi^-$	1394 ± 54	$S_{\pi\pi} = -0.68 \pm 0.10 \pm 0.03$; $C_{\pi\pi} = -0.25 \pm 0.08 \pm 0.02$
$B^0 \rightarrow K^+\pi^-$	5410 ± 91	$\mathcal{A}_{K\pi} = -0.107 \pm 0.016^{+0.006}_{-0.004}$

Table 5: Summary of absolute systematic errors on $\mathcal{A}_{K\pi}$. The total is calculated as the quadrature sum of each contribution. To address the $\mathcal{A}_{K\pi}$ bias due to hadronic interactions of charged kaons with the detector material, we shift the $\mathcal{A}_{K\pi}$ value obtained in the fit by $+0.0050$.

Source	Uncertainty
Material interactions	$+0.0053 -0.0025$
θ_C and dE/dx PDFs	0.0020
Potential MC bias	0.0011
Alternative DIRC parameterization	0.0016
Total	$+0.0060 -0.0037$

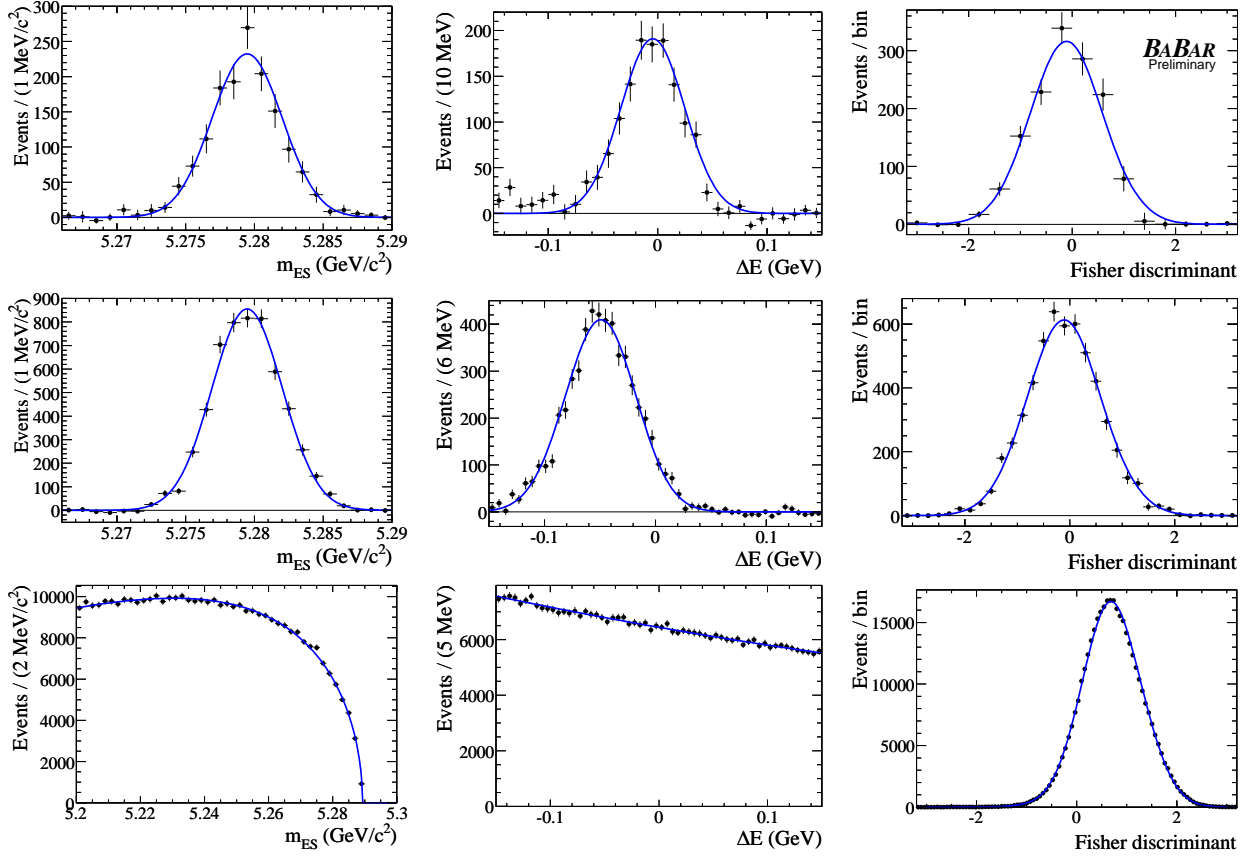


Figure 3: The distributions of (left) m_{ES} , (middle) ΔE , and (right) Fisher discriminant \mathcal{F} : (top) background-subtracted for $B^0 \rightarrow \pi^+\pi^-$ signal, (middle) background-subtracted for $B^0 \rightarrow K^+\pi^-$ signal, (bottom) signal-subtracted for all h^+h^- background candidates in the data. The curves represent the PDFs used in the fit and reflect the fit result. The structure to the left of the signal ΔE peak for $B^0 \rightarrow \pi^+\pi^-$ is consistent with the expected background from other charmless modes, which is negligible above -0.10 GeV.

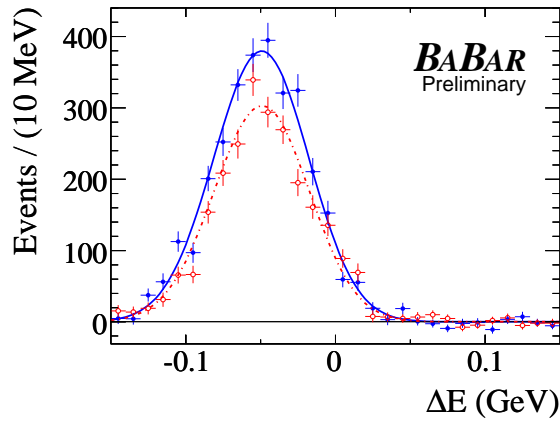


Figure 4: The background-subtracted distribution of ΔE for signal $K^\pm\pi^\mp$ events, comparing (solid) B^0 and (dashed) \bar{B}^0 decays.

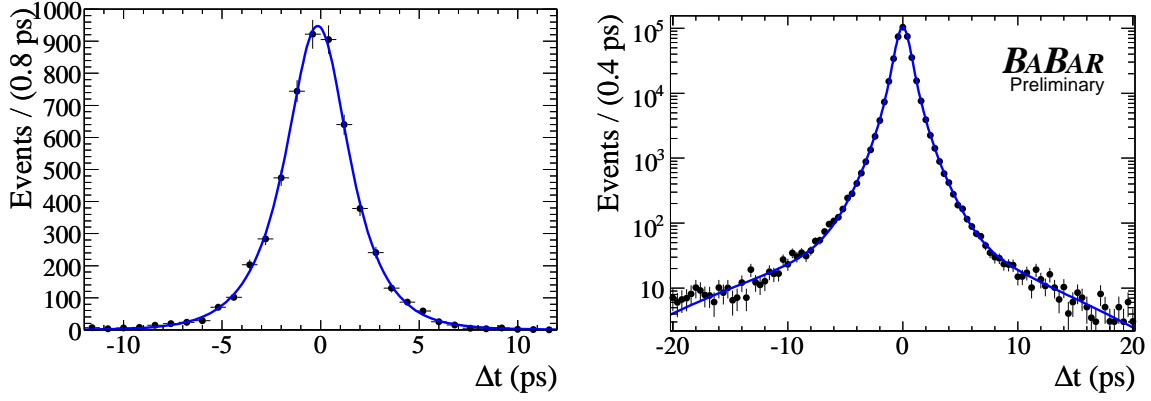


Figure 5: (*Left*) the background-subtracted distribution of Δt for signal $K^\pm\pi^\mp$ and (*right*) the signal-subtracted Δt distribution for background candidates in the data. The curves represent the PDFs used in the fit and reflect the fit result.

Table 6: Summary of systematic uncertainties on $S_{\pi\pi}$ and $C_{\pi\pi}$.

Source	$S_{\pi\pi}$	$C_{\pi\pi}$
DIRC θ_C	0.0064	0.0050
DCH dE/dx	0.0032	0.0037
Signal Δt	0.0199	0.0055
SVT local alignment	0.0004	0.0002
Boost/ z scale	0.0021	0.0013
PEP-II beam spot	0.0028	0.0014
B flavor tagging	0.0146	0.0138
$\Delta m_d, \tau_{B^0}$ [23]	0.0004	0.0017
Potential bias	0.0041	0.0043
Doubly Cabibbo-suppressed decays [35]	0.007	0.016
Total	0.027	0.023

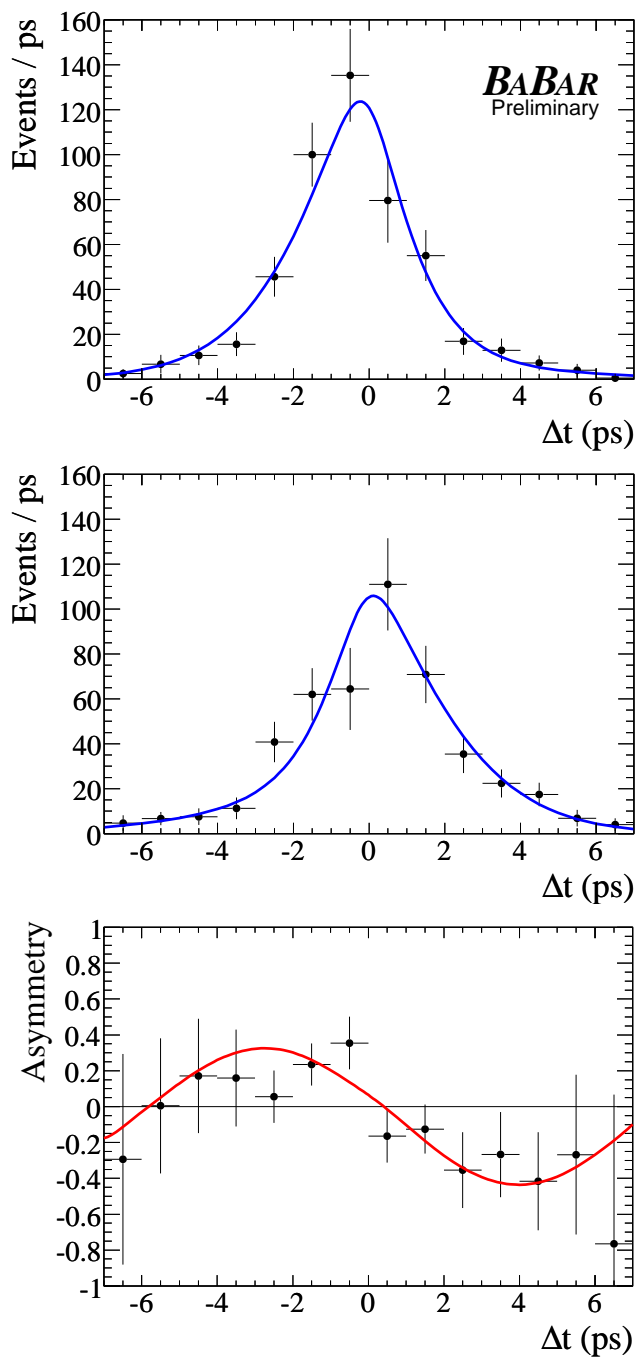


Figure 6: The background-subtracted distributions of Δt for signal $\pi^+\pi^-$ events tagged as (*top*) B^0 or (*middle*) \bar{B}^0 , and (*bottom*) their asymmetry $a(\Delta t)$ (Eq. 1). The curves represent the PDFs used in the fit and reflect the fit result.

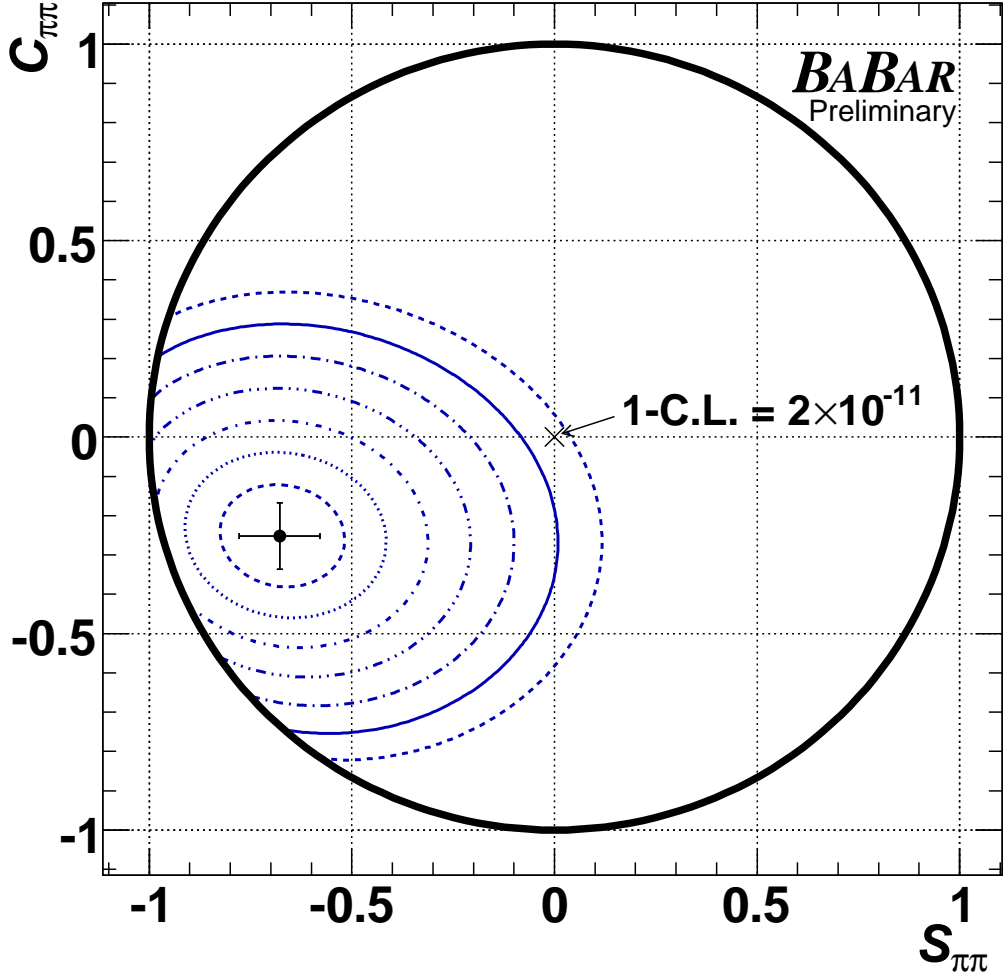


Figure 7: $S_{\pi\pi}$ and $C_{\pi\pi}$ in $B^0 \rightarrow \pi^+\pi^-$: the central values, errors, and confidence-level (C.L.) contours for $1 - \text{C.L.} = 0.317$ (1σ), 4.55×10^{-2} (2σ), 2.70×10^{-3} (3σ), 6.33×10^{-5} (4σ), 5.73×10^{-7} (5σ), 1.97×10^{-9} (6σ) and 2.56×10^{-12} (7σ), calculated from the square root of the change in the value of $-2 \ln \mathcal{L}$ compared with its value at the minimum. The systematic errors are included. The measured value is 6.7σ from the point of no CP violation ($S_{\pi\pi} = 0$, $C_{\pi\pi} = 0$).

Systematic uncertainties for the direct CP asymmetry $\mathcal{A}_{K\pi}$ are listed in Table 5. Here, $\mathcal{A}_{K\pi}$ is the fitted value of the $K^\mp\pi^\pm$ event-yield asymmetry $\mathcal{A}_{K\pi}^{\text{raw}}$ shifted by $+0.005_{-0.003}^{+0.005}$ to account for a bias that arises from the difference between the cross sections of K^+ and K^- hadronic interactions within the *BABAR* detector. We determine this bias from a detailed MC simulation based on GEANT4 [34] version 7.1; it is independently verified with a calculation based on the known material composition of the *BABAR* detector [22] and the cross sections and material properties tabulated in Ref. [23]. The corrected $K^\mp\pi^\pm$ event-yield asymmetry in the background, where no observable CP violation is expected, is consistent with zero: -0.005 ± 0.004 (stat) $_{-0.003}^{+0.005}$ (syst). Systematic uncertainties for the CP asymmetries $S_{\pi\pi}$ and $C_{\pi\pi}$ are listed in Table 6. They are dominated by uncertainties in the parameterization of B -flavor tagging and vertexing, and (for $C_{\pi\pi}$) in the effect of CP violation in B_{tag} [35].

4.3 $B^0 \rightarrow K^0\pi^0$ Results

Results for the $B^0 \rightarrow K^0\pi^0$ decay mode are summarized in Table 2. In Fig. 8, we show $sPlots$ for m_{miss} , m_B , L_2/L_0 , and $|\cos\theta_B^*|$ for signal events, with background distributions shown in the insets.

To compute the systematic error associated with the statistical precision on the parameters of the likelihood function, we shift each parameter by its associated uncertainty and repeat the fit. For Δt and the tagging parameters, the uncertainty is obtained from the fit to the B_{flav} sample, while for the other parameters it is obtained from MC; the total error is obtained by summing the individual contributions in quadrature. This fit systematic also accounts for the limited statistics available to determine the shape of the likelihood function in Eq. 7. We find a systematic error of 1.2 events on the $K_S^0\pi^0$ yield. As an additional systematic error associated with the data–MC agreement of the shape of the signal PDFs, we also quote the largest deviation observed when the parameters of the individual signal PDFs for m_{miss} , m_B , L_2/L_0 , and $\cos\theta_B^*$ are floated in the fit. This gives a systematic error on the yield of 2.5 events. The output values of the PDF parameters are also used to assign a systematic error to the selection efficiency of the cuts on the likelihood variables. Comparing the efficiency in data to that in the MC, we obtain a relative systematic error of 1.5%. We do not assign a systematic uncertainty on the scale of m_{miss} and m_B because we float these variables in the fit. We evaluate the systematic error due to the neglected correlations among fit variables using a set of MC experiments, in which we embed signal events from a full detector simulation with events generated from the background PDFs. Since the shifts are small and only marginally significant, we use the average shift in the yield (+2.2 events) as the associated systematic uncertainty.

We estimate the background from other B decays to be small in the nominal fit. We account for a systematic shift induced on the signal yield by this neglected component by embedding simulated B background events in the data set and evaluating the average shift in the fit result: +5.2 events on the signal yield. We adjust the signal yield accordingly and use half of the shift as a systematic uncertainty.

For the branching fraction, additional systematic errors come from the uncertainty in the selection efficiency, the counting of $B\bar{B}$ pairs in the data sample (1.1%), and the branching fractions in the B^0 decay chain, $\mathcal{B}(K_S^0 \rightarrow \pi^+\pi^-) = 0.6920 \pm 0.0005$ and $\mathcal{B}(\pi^0 \rightarrow \gamma\gamma) = 0.98798 \pm 0.00032$ [23]. The systematic uncertainties are summarized in Table 7.

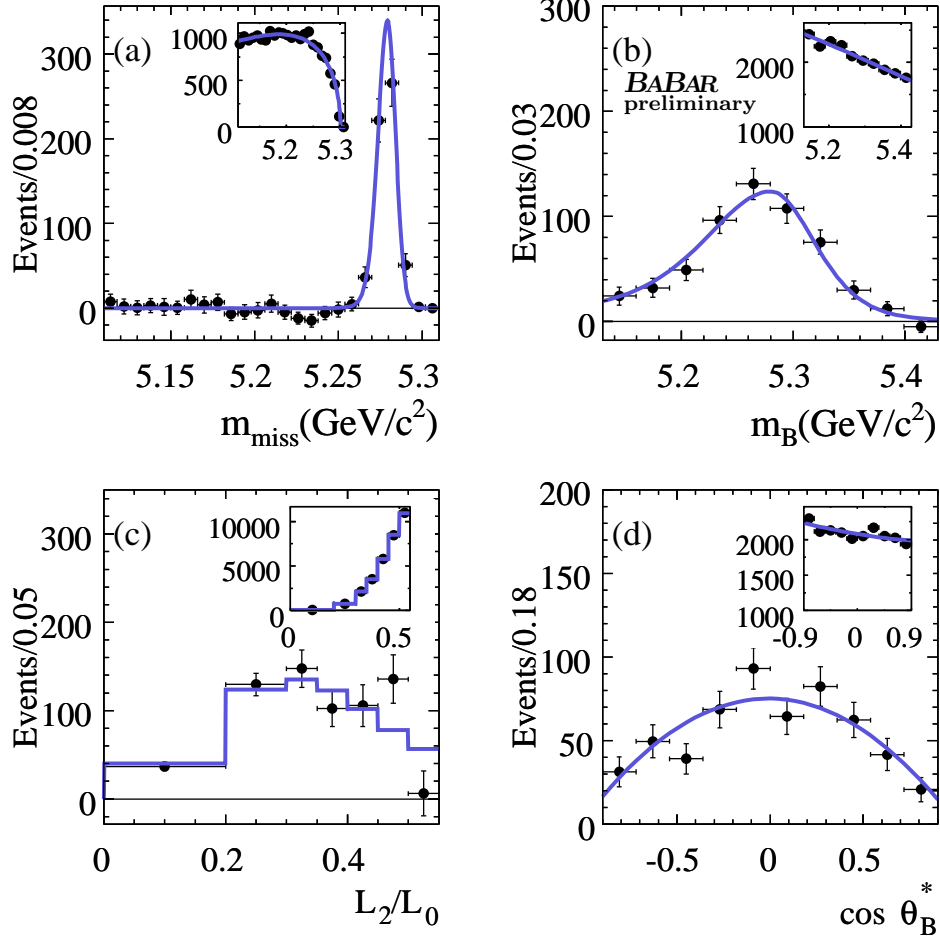


Figure 8: Distributions of (a) m_{miss} , (b) m_B , (c) L_2/L_0 , (d) $\cos\theta_B^*$ for background-subtracted events in the $B^0 \rightarrow K_s^0\pi^0$ sample. The solid curves represent the shapes of signal PDFs as obtained from the M.L. fit. The insets show the distributions and PDFs for signal-subtracted data.

Table 7: Summary of dominant contributions to the systematic error on the measurement of $\mathcal{B}(B^0 \rightarrow K^0\pi^0)$

		$\sigma_{\text{syst}}(\mathcal{B})/\mathcal{B}$ (%)
Efficiencies	π^0 efficiency	3.0
	K_s^0 efficiency	0.5
	Cut on likelihood variables	1.5
Yield	stat. precision on PDF parameters	0.22
	Shape of signal PDFs	0.45
	$B\bar{B}$ background	0.47
	Correlations among likelihood variables	0.40
Normalization	Resolution function	0.49
	Number of $B\bar{B}$ pairs	1.1
Total		3.7

5 CONCLUSIONS

The CP -asymmetry and branching-fraction results described in this paper are:

$$\begin{aligned}
 S_{\pi\pi} &= -0.68 \pm 0.10 \pm 0.03, \\
 C_{\pi\pi} &= -0.25 \pm 0.08 \pm 0.02, \\
 \mathcal{A}_{K\pi} &= -0.107 \pm 0.016_{-0.004}^{+0.006}, \\
 C_{\pi^0\pi^0} &= -0.43 \pm 0.26 \pm 0.05, \\
 \mathcal{B}(B^0 \rightarrow \pi^0\pi^0) &= (1.83 \pm 0.21 \pm 0.13) \times 10^{-6}, \\
 \mathcal{B}(B^0 \rightarrow K^0\pi^0) &= (10.1 \pm 0.6 \pm 0.4) \times 10^{-6}.
 \end{aligned}$$

We combine $\mathcal{B}(B^0 \rightarrow \pi^0\pi^0)$ with the branching fractions $\mathcal{B}(B^0 \rightarrow \pi^+\pi^-) = (5.5 \pm 0.4 \pm 0.3) \times 10^{-6}$ and $\mathcal{B}(B^\pm \rightarrow \pi^\pm\pi^0) = (5.02 \pm 0.46 \pm 0.29) \times 10^{-6}$ previously measured by *BABAR* [13,14] to evaluate the constraints on both the penguin contribution to α and on the CKM angle α itself. Constraints are evaluated by scanning the parameters of interest, $|\Delta\alpha_{\pi\pi}| = |\alpha - \alpha_{\text{eff}}|$ and α , and then calculating the χ^2 for the five amplitudes (A^{+0} , A^{+-} , A^{00} , \bar{A}^{+-} , \bar{A}^{00}) from our measurements and the isospin-triangle relations [8]. The χ^2 is converted to a confidence level (C.L.) as shown in Fig. 9. The upper bound on $|\Delta\alpha_{\pi\pi}|$ is 43° at the 90% C.L., and the range $[23^\circ, 67^\circ]$ in α is excluded at the 90% C.L. If we consider only the solution preferred in the SM [37], α is in the range $[71^\circ, 109^\circ]$ at the 68% C.L. Somewhat more restrictive new constraints on α have been found in the measurements of $B \rightarrow \rho\rho$ and $B^0 \rightarrow (\rho\pi)^0$ decays [38].

We have also presented an improved measurement of the CP -violating charge asymmetry $\mathcal{A}_{K\pi}$ in the $B^0 \rightarrow K^+\pi^-$ decay. We observe direct CP violation in $B^0 \rightarrow K^+\pi^-$ with a significance of 6.1σ . Ignoring color-suppressed tree amplitudes, the charge asymmetries in $K^+\pi^-$ and $K^+\pi^0$ should be equal (see Gronau and Rosner in Ref. [21]), which has not been supported by recent *BABAR* and Belle data [5, 7, 13]. These results might indicate a large color-suppressed amplitude, an enhanced electroweak penguin, or possibly new-physics effects [39].

Finally, we have presented an improved measurement of $\mathcal{B}(B^0 \rightarrow K^0\pi^0)$. From the rate sum-rule prediction [21] $2\mathcal{B}(K^0\pi^0)^{\text{sr}} = \mathcal{B}(K^+\pi^-) + \frac{\tau_0}{\tau_+}[\mathcal{B}(K^0\pi^+) - 2\mathcal{B}(K^+\pi^0)]$ and the currently published results for the other three $B \rightarrow K\pi$ modes, we find the sum-rule prediction to be $\mathcal{B}(B^0 \rightarrow K^0\pi^0)^{\text{sr}} = (8.4 \pm 0.8) \times 10^{-6}$, which is consistent with our new experimental result.

6 ACKNOWLEDGMENTS

We are grateful for the extraordinary contributions of our PEP-II colleagues in achieving the excellent luminosity and machine conditions that have made this work possible. The success of this project also relies critically on the expertise and dedication of the computing organizations that support *BABAR*. The collaborating institutions wish to thank SLAC for its support and the kind hospitality extended to them. This work is supported by the U.S. Department of Energy and National Science Foundation, the Natural Sciences and Engineering Research Council (Canada), the Commissariat à l’Energie Atomique and Institut National de Physique Nucléaire et de Physique des Particules (France), the Bundesministerium für Bildung und Forschung and Deutsche Forschungsgemeinschaft (Germany), the Istituto Nazionale di Fisica Nucleare (Italy), the Foundation for Fundamental Research on Matter (The Netherlands), the Research Council of Norway, the Ministry of Education and Science of the Russian Federation, Ministerio de Educación y Ciencia (Spain),

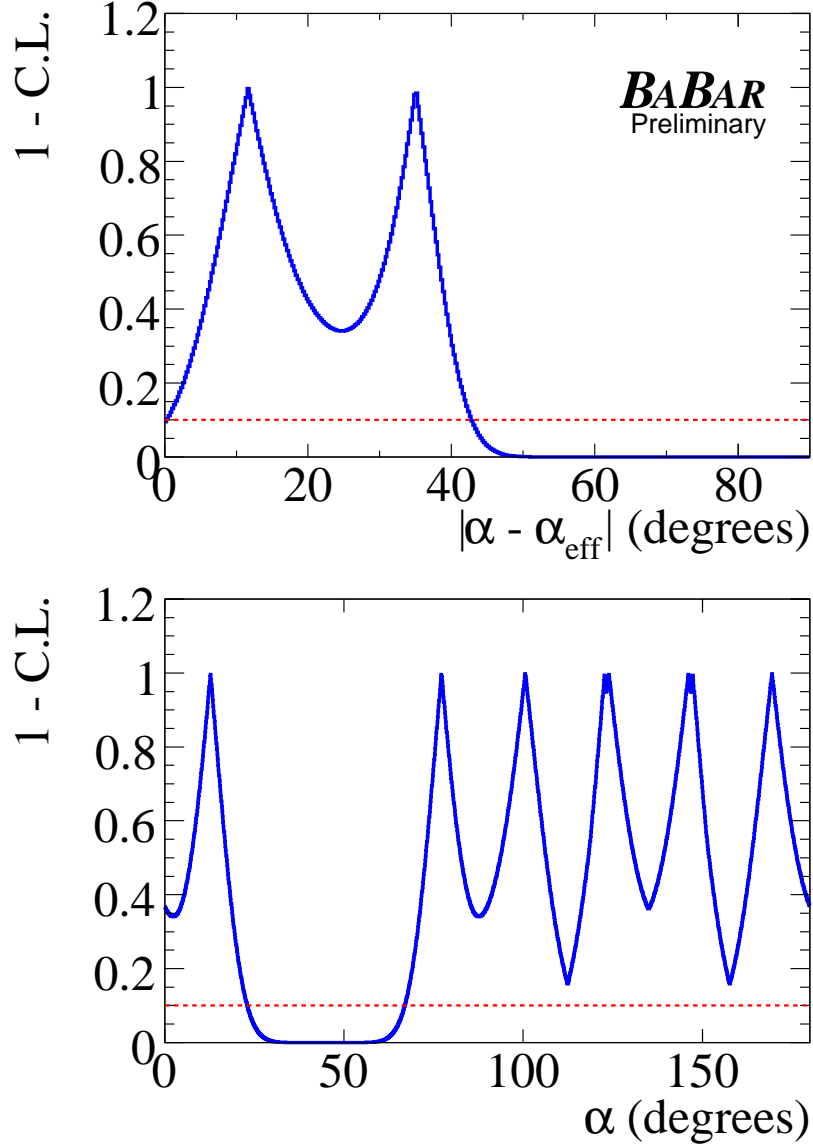


Figure 9: (*Top*) constraint on the angle $\Delta\alpha_{\pi\pi} = \alpha - \alpha_{\text{eff}}$, expressed as one minus the confidence level (C.L.), as a function of $|\Delta\alpha_{\pi\pi}|$. We find an upper bound on $|\Delta\alpha_{\pi\pi}|$ of 43° at the 90% C.L. (*Bottom*) constraint on the CKM angle α expressed as $1 - \text{C.L.}$. There are eight peaks, two of them nearly merged, corresponding to an eight-fold ambiguity in the extraction of α ; four solutions are from the value and sign of $\Delta\alpha_{\pi\pi}$, which is doubled due to the trigonometric reflections between α_{eff} and $\pi/2 - \alpha_{\text{eff}}$. We exclude the range $[23^\circ, 67^\circ]$ in α at the 90% C.L. Only the isospin-triangle relations and the expressions in Eq. 1 are used in this constraint. The point $\alpha = 0$, which corresponds to no CP violation, and the values of α near 0 or π can be excluded with additional physics input [13,36].

and the Science and Technology Facilities Council (United Kingdom). Individuals have received support from the Marie-Curie IEF program (European Union) and the A. P. Sloan Foundation.

References

- [1] A. Carter and A. I. Sanda, Phys. Rev. Lett. **45**, 952 (1980); M. Bander, D. Silverman, and A. Soni, Phys. Rev. Lett. **43**, 242 (1979).
- [2] N. Cabibbo, Phys. Rev. Lett. **10**, 531 (1963); M. Kobayashi and T. Maskawa, Prog. Theor. Phys. **49**, 652 (1973).
- [3] B. Aubert *et al.* (BABAR Collaboration), Phys. Rev. Lett. **99**, 171803 (2007); B. Aubert *et al.* (BABAR Collaboration), Phys. Rev. Lett. **98**, 031801 (2007); K.-F. Chen *et al.* (Belle Collaboration), Phys. Rev. Lett. **98**, 031802 (2007); H. Sahoo *et al.* (Belle Collaboration), Phys. Rev. D **77**, 091103 (2008).
- [4] H. Ishino *et al.* (Belle Collaboration), Phys. Rev. Lett. **98**, 211801 (2007).
- [5] B. Aubert *et al.* (BABAR Collaboration), Phys. Rev. Lett. **99**, 021603 (2007).
- [6] The use of charge-conjugate modes is implied throughout this paper unless otherwise noted.
- [7] S.-W. Lin, Y. Unno, W.-S. Hou, P. Chang *et al.* (Belle Collaboration), Nature **452**, 332 (2008).
- [8] J. Charles *et al.* (CKMfitter Group), Eur. Phys. J. C **41**, 1 (2005).
- [9] M. Bona *et al.* (UTfit Collaboration), JHEP **0507**, 028 (2005).
- [10] M. Bona *et al.* (UTfit Collaboration), Phys. Rev. Lett. **97**, 151803 (2006); M. Bona *et al.* (UTfit Collaboration), JHEP **0803**, 049 (2008).
- [11] M. Gronau and D. London, Phys. Rev. Lett. **65**, 3381 (1990).
- [12] M. Beneke and M. Neubert, Nucl. Phys. B **675**, 333 (2003); C. W. Bauer, D. Pirjol, I. Z. Rothstein, and I. W. Stewart, Phys. Rev. D **70**, 054015 (2004); Y. Y. Keum, H. n. Li, and A. I. Sanda, AIP Conf. Proc. **618**, 229 (2002);
M. Ciuchini, E. Franco, G. Martinelli, M. Pierini, and L. Silvestrini, Phys. Lett. B **515**, 33 (2001).
- [13] B. Aubert *et al.* (BABAR Collaboration), Phys. Rev. D **76**, 091102 (2007).
- [14] B. Aubert *et al.* (BABAR Collaboration), Phys. Rev. D **75**, 012008 (2007).
- [15] B. Aubert *et al.* (BABAR Collaboration), Phys. Rev. Lett. **97**, 171805 (2006);
- [16] B. Aubert *et al.* (BABAR Collaboration), Phys. Rev. D **77**, 012003 (2008);
- [17] K. Abe *et al.* (Belle Collaboration), Phys. Rev. Lett. **98**, 181804 (2007); K. Abe *et al.* (Belle Collaboration), Phys. Rev. Lett. **99**, 121601 (2007).
- [18] A. Bornheim *et al.* (CLEO Collaboration), Phys. Rev. D **68**, 052002 (2003) [Erratum-ibid. D **75**, 119907 (2007)].

- [19] A. J. Buras and R. Fleischer, Eur. Phys. J. C **16**, 97 (2000); A. J. Buras, R. Fleischer, S. Recksiegel, and F. Schwab, Phys. Rev. Lett. **92**, 101804 (2004); A. J. Buras, R. Fleischer, S. Recksiegel, and F. Schwab, Nucl. Phys. B **697**, 133 (2004).
- [20] M. Gronau and J. L. Rosner, Phys. Lett. B **572**, 43 (2003); T. Yoshikawa, Phys. Rev. D **68**, 054023 (2003); V. Barger, C. W. Chiang, P. Langacker, and H. S. Lee, Phys. Lett. B **598**, 218 (2004); S. Mishima and T. Yoshikawa, Phys. Rev. D **70**, 094024 (2004); Y.-L. Wu and Y.-F. Zhou, Phys. Rev. D **71**, 021701 (2005).
- [21] M. Gronau, Phys. Lett. B **627**, 82 (2005); M. Gronau and J. L. Rosner, Phys. Rev. D **59**, 113002 (1999); H. J. Lipkin, Phys. Lett. B **445**, 403 (1999); C. W. Bauer, I. Z. Rothstein, and I. W. Stewart, Phys. Rev. D **74**, 034010 (2006).
- [22] B. Aubert *et al.* (BABAR Collaboration), Nucl. Instrum. Methods Phys. Res. A **479**, 1 (2002).
- [23] W.-M. Yao *et al.* (Particle Data Group), J. Phys. G **33**, 1 (2006).
- [24] J. D. Bjorken and S. J. Brodsky, Phys. Rev. D **1**, 1416 (1970).
- [25] S. Brandt *et al.*, Phys. Lett. **12**, 57 (1964); E. Farhi, Phys. Rev. Lett. **39**, 1587 (1977).
- [26] G. C. Fox and S. Wolfram, Phys. Rev. Lett. **41**, 1581 (1978).
- [27] B. Aubert *et al.* (BABAR Collaboration), Phys. Rev. Lett. **94**, 161803 (2005).
- [28] B. Aubert *et al.* (BABAR Collaboration), Phys. Rev. D **66**, 032003 (2002).
- [29] The function is $f(x) \propto x\sqrt{1-x^2} \exp[-\zeta(1-x^2)]$, where the slope ζ is a fit parameter and $x = m_{ES}/E_b^*$; H. Albrecht *et al.* (ARGUS Collaboration), Z. Phys. C **48**, 543 (1990).
- [30] B. Aubert *et al.* (BABAR Collaboration), Phys. Rev. D **71**, 111102 (2005).
- [31] B. Aubert *et al.* (BABAR Collaboration), Phys. Rev. D **77**, 012003 (2008).
- [32] M. Pivk and F. R. Le Diberder, Nucl. Instrum. Methods Phys. Res., Sect. A **555**, 356 (2005).
- [33] B. Aubert *et al.* (BABAR Collaboration), BABAR-PUB-08/041.
- [34] S. Agostinelli *et al.* (GEANT4 Collaboration), Nucl. Instrum. Methods Phys. Res., Sect. A **506**, 250 (2003).
- [35] O. Long, M. Baak, R. N. Cahn, and D. Kirkby, Phys. Rev. D **68**, 034010 (2003).
- [36] M. Bona *et al.* (UTfit Collaboration), Phys. Rev. D **76**, 014015 (2007).
- [37] M. Gronau and J. L. Rosner, Phys. Lett. B **651**, 166 (2007).
- [38] B. Aubert *et al.* (BABAR Collaboration), Phys. Rev. Lett. **97**, 261801 (2006); B. Aubert *et al.* (BABAR Collaboration), Phys. Rev. D **76**, 052007 (2007); B. Aubert *et al.* (BABAR Collaboration), Phys. Rev. D **76**, 012004 (2007); B. Aubert *et al.* (BABAR Collaboration), arXiv:0807.4977 [hep-ex].
- [39] W. S. Hou, M. Nagashima, and A. Soddu, Phys. Rev. Lett. **95**, 141601 (2005); R. Fleischer, S. Recksiegel, and F. Schwab, Eur. Phys. J. C **51**, 55 (2007).